

# Calculations of X-ray Emission Spectra of Molecules and Surface Adsorbates by Means of Density Functional Theory

L. Triguero,<sup>†</sup> L. G. M. Pettersson,<sup>†</sup> and H. Ågren<sup>\*,‡</sup>

FYSIKUM, University of Stockholm, Box 6730, S-113 85 Stockholm, Sweden, and Institute of Physics and Measurement Technology, Linköping University, S-58183 Linköping, Sweden

Received: January 20, 1998

In the present study we apply density functional theory (DFT) to calculate nonresonant X-ray emission (XE) spectra of free and chemisorbed molecules. Both ground state frozen orbital and transition potential relaxed orbital procedures are investigated for the calculation of X-ray emission energies and intensities. A code implementation of these proposals has been applied to the free and surface-adsorbed carbon monoxide, ethylene, and benzene molecules and to surface-adsorbed atomic nitrogen. The results are analyzed in comparison with experimental data and with calculations using Hartree–Fock theory. Different standard exchange–correlation functionals have been discussed. The quality of the computed DFT-level XE spectra is comparable to what is obtained using Hartree–Fock theory for intensities of the free molecules but improves, in general, the description of the spectra for the surface adsorbates. The best experimental comparison is obtained when putting the X-ray emission spectra on a common energy scale using the valence transition potentials for energies and the frozen ground state wave function for the intensities.

## I. Introduction

The local probe character of X-ray emission (XE) spectra has opened new paths to understand the bonding of molecules to surfaces. Recent experimental work in this field has led to the proposal of a new orbital model for such bonding, which to some extent contrasted well-recognized points of views<sup>1,2</sup> such as the Blyholder model of chemisorption. Apart from experimentally based modeling, there is currently also a surge to use electronic structure theory, both to analyze the bonding and to compute X-ray spectra of surface adsorbates, with the idea to combine the analysis of the spectra and of the bonding to provide better and more reliable conclusions. In contrast to X-ray absorption, nonresonant X-ray emission applied to surface adsorbates is a relatively new technique and rather little has therefore been accomplished so far by theory and computation. In the present work we take advantage of the general applicability of density functional theory (DFT) and propose a simple modification thereof for studying X-ray emission spectra. Such an attempt conceivably also improves the problem of uncorrelated reference states in the *ab initio* molecular orbital approaches and the problem of obtaining proper ground state charge transfer between the surface and the adsorbate. The proposed computational technique uses the *ground state* orbitals in the evaluation of transition intensities and a transition potential calculation of the valence orbital binding energies to generate the full XE spectra; initial state (core-hole) and final state (valence-hole) relaxation are thus both included in the calculations of the excitation energies, while neither initial nor final state relaxation is included in the calculation of the intensities.

Recent works on molecules<sup>3–5</sup> and surface adsorbates<sup>6</sup> have demonstrated that DFT in a transition potential approach (DFT-TP) is a viable way to compute near-edge X-ray absorption (NEXAFS) spectra. This led the authors to propose that it can

be extended to X-ray emission,<sup>6</sup> which carries many features that are complementary to NEXAFS in that it images the electronic structure of the ground state, i.e., the occupied rather than the unoccupied levels. It is the purpose of the present paper to make a closer investigation of this proposal.

We choose a set of molecules, CO, C<sub>2</sub>H<sub>4</sub>, C<sub>6</sub>H<sub>6</sub>, which are also accessible by the Hartree–Fock method and by experiment. For CO and C<sub>2</sub>H<sub>4</sub>, we have computed the X-ray emission spectra both for the free and chemisorbed species, while for C<sub>6</sub>H<sub>6</sub> we have studied XE spectra for the adsorbed molecule on the Cu(110) surface. We also include the N/Cu(100) system to represent atomic surface adsorbates, so as to obtain a proper comparison of the two approaches. The main purpose of the present work is thus to evaluate the DFT method applied to X-ray emission spectra for both free and chemisorbed molecules; a full analysis of the spectra displayed here will be given elsewhere.<sup>6–8</sup>

## II. Method and Calculations

We consider the orbital-based Kohn–Sham (KS) equations

$$H_{\text{KS}}\phi_i = \epsilon_i\phi_i \quad (1)$$

where  $H_{\text{KS}}$  is the local operator with the exchange–correlation potential  $V_{\text{xc}}[\rho(r)]$

$$H_{\text{KS}} = -\frac{1}{2}\nabla^2 - \sum_N \frac{Z_N}{|r_N - r|} + \int \frac{\rho(r')}{|r - r'|} dr' + V_{\text{xc}}[\rho(r)] \quad (2)$$

and

$$\rho(r) = \sum_i^{\text{occ}} \sum_s^{\text{spin}} n_i |\phi(\vec{r}, s)|^2 \quad (3)$$

and utilize the implementation of this equation in the deMon

<sup>†</sup> University of Stockholm.

<sup>‡</sup> Linköping University.

program.<sup>9</sup> Two different approaches to generate the XE spectra will be discussed: either using the optimized ground state Kohn–Sham orbitals in the transition moment calculation or using a transition potential formalism. The transition state<sup>10</sup> with half an electron in the core orbital participating in the X-ray emission plays a special role since the relaxation following ionization of the core electron then is included up to second order<sup>10</sup>

$$E_b(1s) = - \left. \frac{\delta E_0(n_{1s})}{\delta n_{1s}} \right|_{n_{1s}=1/2} \quad (4)$$

The transition potential method is thus useful in cases where Koopman’s theorem fails, as for core ionization, and has been implemented in several MSX<sub>α</sub>, Hartree–Fock, and DFT schemes.<sup>3,4,11–13</sup> In the present study, we investigate two different ways to generate the X-ray emission oscillator strengths and excitation energies. First, we use the Kohn–Sham state optimized for the half-occupied core orbital with binding energy  $-\epsilon_{1s}(n_{1s}^{1/2})$  and where the oscillator strengths are given as  $^{2/3} \langle \phi_{1s}(n_{1s}^{1/2}) | \hat{r} | \phi_i(n_{1s}^{1/2}) \rangle^2$ . The spectral intensities are thus obtained from orthogonal and noninteracting eigenstates of the Kohn–Sham equation (eq 1) while the valence binding energies are approximated by  $-\epsilon_i(n_{1s}^{1/2})$ , which is obtained from a KS optimization with a fractional occupation,  $n_{1s} = 1/2$ , in the 1s orbital while the remaining occupied spin orbitals are populated by one electron each (unrestricted spin orbitals are assumed); this approach will be denoted DFT-TP. Second, we use the frozen orbital approximation (DFT-Frozen), which corresponds to a ground state Kohn–Sham orbital calculation. Here, the oscillator strengths are given by dipole moment transitions between the 1s orbital and the valence orbitals  $\phi_i(^{2/3} \langle \phi_{1s} | \hat{r} | \phi_i \rangle^2)$ . The excitation energies are then separately computed using the transition potential approach for each of the valence orbitals,  $\epsilon_i(n_{1s}^{1/2})$ . The core ionization potentials obtained from the  $n_{1s}^{1/2}$  transition potential are notoriously ca. 1.5–2 eV larger than the “ΔSCF” Kohn–Sham energies and the experimental value (see ref 6 for details). The errors in the  $\epsilon_{1s}(n_{1s}^{1/2})$  binding energy can be assigned to higher order contributions to the core relaxation energy not covered by  $n_{1s}^{1/2}$  transition potential theory but which are included in a fully relaxed “ΔSCF” Kohn–Sham calculation; thus, the core ionization potentials (IPs) reported in both approaches are computed using this ΔSCF procedure.

XE spectroscopy is an element-specific local probe of the character of the occupied molecular orbitals. By choosing the energy of the initial exciting photon, one may select a particular site in a multicentered molecule, e.g., the 1s core hole may be created specifically at the carbon atom in the CO molecule. Irrespective of which initial core-hole state is created, the subsequent radiative decay yields a common set of valence-hole final states. A simple theoretical treatment where the full spectrum, for a given initial core-hole state, is generated from a single calculation is desirable but cannot be implemented within the transition potential formalism for a heteronuclear molecule due to the different effects on the valence orbital structure from core holes at different sites; this follows from the  $Z + 1$  approximation. If one normalizes the XE transition energies to the core ionization energy (for instance, the experimental one), the transition potential approach with a half-occupied core level will thus give different valence ionization IPs for different core-hole transition states. This means that, for example, the carbon and oxygen XE spectra of CO cannot be put on a common binding energy scale and a separate

transition state calculation must instead be performed for each X-ray transition, something which, as will be shown in the following, is favorable for obtaining accurate transition energies.

In the following the “transition potential approach” denotes a procedure in which we obtain both intensities and valence binding energies from a single optimization of the state with a half-occupied core level at the site of interest, while the core binding energy is obtained from a separate calculation. This procedure results in a dependence on the core hole of the valence binding energies. The DFT “frozen orbital” approach denotes a procedure where the intensities are obtained from the ground state orbitals while valence binding energies are obtained from separate transition state calculations for each valence orbital and the core binding energy is obtained from a “ΔSCF” Kohn–Sham calculation. In the latter approach the final and initial state relaxation are thus included in the calculation of energies, but no effect of relaxation is included in the calculation of the intensities for the presented spectra. The two approaches are compared in the following. The role of relaxation is shown for the C<sub>6</sub>H<sub>6</sub>/Cu<sub>13</sub> system in Figure 6 and discussed in section III.D. A more general discussion on the role of relaxation for XES of surface adsorbates is given in section III.F.

Calculations of the X-ray emission spectra are carried out with the deMon program,<sup>9</sup> which implements orbital-based density functional theory, and with the DISCO program<sup>14</sup> for Hartree–Fock (HF) calculations. Similar HF calculations have been carried out earlier for the CO, atomic nitrogen, and C<sub>6</sub>H<sub>6</sub> adsorbates in refs 7, 8, and 15, and we refer to these papers for detailed descriptions of such calculations. For the ethylene molecule, we used for carbon the triple- $\zeta$  valence polarization (TZVP)<sup>16</sup> in a generalized [4s,3p] contraction and with one added d function, while for hydrogen, the primitive (5s) basis set from ref 17 was used, augmented with one p function and contracted to [3s,1p]. These basis sets were used both for the optimization of the geometry<sup>18</sup> and for the determination of the spectra. The following functionals have been applied in the DFT-based calculations: the gradient corrections due to Perdew and Wang (PW86 and PW91)<sup>19–22</sup> for the exchange and correlation potential and to Becke (B)<sup>23</sup> for the exchange part, together with the Perdew (P86)<sup>20,21</sup> for the correlation functional. The LDA calculations were performed using the VWN potential.<sup>24</sup>

The calculations of XE spectra of the chemisorbed molecules were carried out using cluster models of the metal surface and with all structural degrees of freedom of the adsorbates optimized using energy gradients; the metal atoms in the cluster were frozen in their bulk positions. Clusters employed in this work are similar to those in a companion paper on NEXAFS.<sup>6</sup> Thus for the smaller copper cluster models (up to Cu<sub>18</sub>) in the DFT framework, the copper atoms were described at the all-electron level using the Wachters<sup>25</sup> basis set in an [8s5p3d] contraction with one diffuse p and one d function added. The all-electron cluster description was used for all applications to ethylene and benzene chemisorption, including the geometry optimization of the ethylene at the di- $\sigma$  adsorption site on Cu(110) as well as for the benzene on Cu(110),<sup>18</sup> and for the optimization of CO on a Cu<sub>14</sub> cluster modeling the on-top site of Cu(100). For the larger cluster models, e.g., Cu<sub>50</sub> for CO/Cu(100) and Cu<sub>61</sub> for N/Cu(100), the central Cu<sub>5</sub> subunit was described at the all-electron level and the surrounding atoms were described using a one-electron effective core-potential (ECP) model developed by Wahlgren and co-workers.<sup>26</sup> The core, including the 3d shell, is thus described by a static potential, which includes the effects of relaxation and polariza-

**TABLE 1: Comparison of Carbon and Oxygen Relative X-ray Intensities of CO at Different Levels of Approximations**

level transition	HF <sup>a</sup> relax.	HF <sup>a</sup> froz	MCSCF <sup>b</sup> relax.	CI <sup>c</sup> relax.	DFT TP	DFT froz	DFT expt <sup>d</sup>
C1s <sup>-1</sup> -5σ <sup>-1</sup>	1.11	1.10	0.82	0.850	0.77	0.87	0.86
C1s <sup>-1</sup> -1π <sup>-1</sup>	1.0	1.0	1.0	1.0	1.0	1.0	1.0
C1s <sup>-1</sup> -4σ <sup>-1</sup>	0.10	0.10	0.06	0.054	0.04	0.06	
C1s <sup>-1</sup> -3σ <sup>-1</sup>	0.33		0.19	0.189 <sup>e</sup>	0.24		
O1s <sup>-1</sup> -5σ <sup>-1</sup>	0.10	0.09	0.09	0.074	0.08	0.13	0.13
O1s <sup>-1</sup> -1π <sup>-1</sup>	1.0	1.0	1.0	1.0	1.0	1.0	1.0
O1s <sup>-1</sup> -4σ <sup>-1</sup>	0.42	0.32	0.32	0.322	0.38	0.39	0.24
O1s <sup>-1</sup> -3σ <sup>-1</sup>	0.05		0.04	0.023 <sup>e</sup>	0.023		

<sup>a</sup> Hartree–Fock results from ref 42. <sup>b</sup> Separate state MCSCF calculations from ref 41 (large basis set). <sup>c</sup> CI calculations with nonorthogonal molecular orbitals from ref 28 (large basis set). <sup>d</sup> Experimental results from ref 29. <sup>e</sup> Summed over four correlation split states 28.

**TABLE 2: Valence Orbital and X-ray Emission Energies (eV) for Free CO Computed Using Different Approaches<sup>a</sup>**

orbital	expt	ε <sub>i</sub> (n <sub>i</sub> <sup>1/2</sup> )		Δ	KT	ΔSCF	ΔMCPF <sup>b</sup>	
		C	O					
5σ	14.0	14.1	15.2	14.3	-0.9	15.1	13.4	13.8
1π	16.8	17.4	17.8	18.2	-0.4	17.4	15.2	16.8
4σ	19.7	19.9	20.2	20.5	-0.3	21.9	19.6	21.0

CO Gas-Phase, X-ray Emission Energies

orbital	expt <sup>c</sup>		IP <sub>1s</sub> -  ε <sub>i</sub> (n <sub>i</sub> <sup>1/2</sup> )  <sup>d</sup>	
	C	O	C	O
5σ	282.1	528.1	282.5	528.8
1π	279.0	525.0	279.7	526.0
4σ	276.4	522.3	276.8	523.1

<sup>a</sup> |ε<sub>i</sub>(n<sub>i</sub><sup>1/2</sup>)| indicates the separate transition potential used for each valence orbital. C and O indicate valence binding energies obtained from C(1s) and O(1s) transition potentials, respectively, while Δ gives the difference between the two. KT stands for the Koopman’s theorem value at the Hartree–Fock level. <sup>b</sup> MCPF = Modified coupled pair functional method.<sup>43</sup> <sup>c</sup> Experimental values from ref 29. <sup>d</sup> IP<sub>1s</sub><sup>C</sup> = 296.5 eV and IP<sub>1s</sub><sup>O</sup> = 542.8 eV (see ref 6).

tion of the 3d orbitals, but which only treats the 4s valence electrons explicitly.

### III. Results and Discussion

**A. Free CO.** The majority of theoretical analyses of X-ray emission spectroscopy (XES) investigations are carried out using the frozen orbital one-center model, which provides the “interpretability” of the X-ray emission experiment as a local probe of the electronic structure. Beyond this model, soft X-ray emission spectra of molecules have been analyzed at several more sophisticated levels, including also core relaxation and electron correlation effects.<sup>27</sup> As for NEXAFS, CO stands as a prototype for the remarkable features of XES. With two core-hole derived spectra, the XES intensities follow localization of the molecular orbitals. A collection of previous results for the CO molecule is given in Table 1 and compared with intensities obtained from the two DFT approaches: the DFT-TP method assuming an ε<sub>1s</sub>(n<sub>1s</sub><sup>1/2</sup>) transition state (1s denoting either the oxygen or the carbon core orbital) and the DFT-Frozen approach with the intensities calculated using the ground state orbitals. Indeed the results are not very different from those obtained with the MCSCF/CI methods.

Table 2 lists the XES transition energies renormalized to a valence binding energy scale. The energies are obtained from the two ε<sub>1s</sub>(n<sub>1s</sub><sup>1/2</sup>) transition potentials and from separate valence

ε<sub>i</sub>(n<sub>i</sub><sup>1/2</sup>) transition potentials. One notes that the latter results seem to come out somewhat better, both with respect to absolute and relative valence energies. One also notes that the two (C1s and O1s) core transition potentials can give different valence energies. The valence IPs agree within a few tenths of an electronvolt, and the X-ray emission energies (difference of core and valence IPs) are all within 1 eV. The 3σ level is subject to a strong correlation breakdown (a prediction of four major breakdown states is given in ref 28), and such “static” correlation effects are, in principle, unaccounted for by DFT approaches (inner valence levels are mainly of local s-character and therefore are quite weak in XE spectra of first-row compounds).

When comparing with the absolute X-ray transition energies, it is essential to use corrections to the DFT-TP value by the Kohn–Sham optimized 1s (ΔSCF) ionization potential.<sup>6</sup> If so, the agreement for absolute XE energies also becomes very good. For a comparison with experiment of absolute XE energies on a subelectronvolt scale, one should also take into account that the vertical (center-of-gravity) X-ray emission energies differ from subtracted vertical core and valence ionization potentials as measured by X-ray and ultraviolet photoelectron spectroscopy (UPS), since the vibrational progressions differ for the different processes. For instance, the apparent vertical energy for the C1s–1π transition in CO differs between the two spectroscopies by almost 1 eV.<sup>29</sup> Furthermore, lifetime vibrational interference effects shift and distort the band profiles, especially when the lifetime of the core-hole state and the vibrational periods are of the same order of magnitude.

**B. CO/Cu(100).** The published XE spectra of CO on copper surfaces show some salient features between 3 and 13 eV on a binding energy scale referring to the Fermi level<sup>30,31</sup> (273–283 and 520–530 eV on a transition energy scale for the carbon and oxygen spectra, respectively). The oxygen spectrum retains a three-band feature with some structure in the middle band; the carbon spectrum has a composite double-band feature. The ability to switch detection directions, from surface normal to grazing angles, has made it possible to assign π and σ character of the emitting states. The surface-induced shifts of the spectra accord well with corresponding XPS and UPS shifts.<sup>32</sup> The intensity at the Fermi level is close to zero in both spectra in contrast to UPS, indicating little adsorbate p-localization at this part and contrasting the resonance model interpretation of the adsorbate–substrate bonding.<sup>30</sup>

Figures 1–3 and Table 3 compare the computed O1s and C1s XES spectra using different levels of approximation for free and chemisorbed CO, where two models, CO/Cu<sub>14</sub> and CO/Cu<sub>50</sub>, of the on-top chemisorption site for CO/Cu(100) are used. We first note that energetically a good cluster convergence and good agreement with experiment<sup>31</sup> are obtained for both the DFT-TP and DFT-Frozen approaches. The relative positions of the three 1π, 5σ, and 4σ bands are well reproduced, and even the absolute positions on the common binding energy scale are accurate to within 1 eV. Concerning intensities, one notes the dominance of the 1π transition in both spectra, actually being more dominant than that for free CO; this is also observed in the experiment. The 4σ orbital is represented only in the oxygen spectrum. The 1π to 4σ (oxygen spectrum) and 1π to 5σ (carbon spectrum) ratios seem well reproduced in all cases (free and chemisorbed CO). The O1s–5σ transition seems, on the other hand, to be strongly enhanced in going from the free to the chemisorbed molecule in a way that is unaccounted for by the DFT-TP calculations; the computed spectral intensities for the 4σ, 1π, and 5σ bands change surprisingly little in going from free CO to CO/Cu<sub>50</sub>. Turning to the corresponding intensity

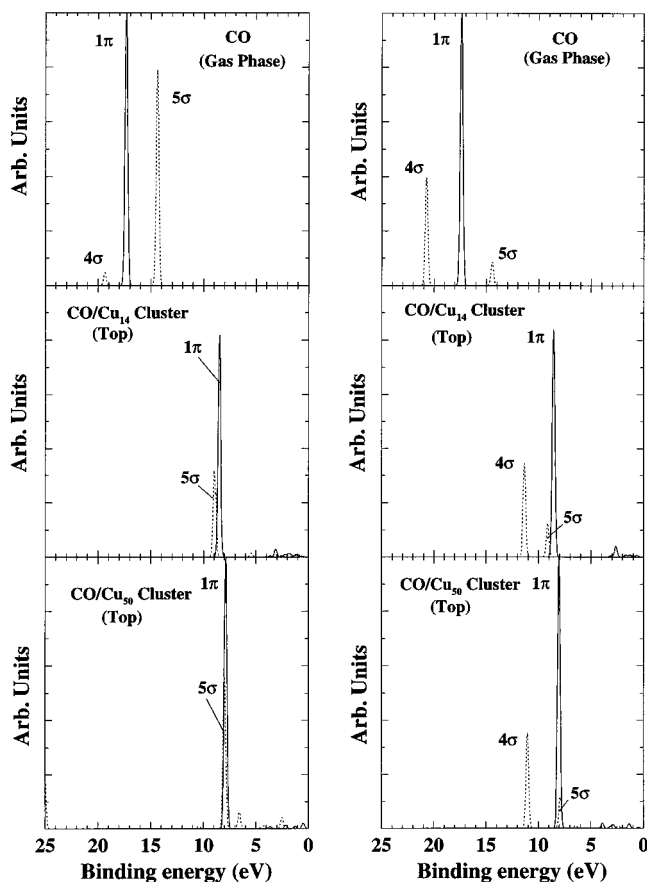


**Figure 1.** Theoretical C(1s) and O(1s) XES spectra computed from DFT-TP with Cu–C distance of  $3.51 a_0$  and PD91 exchange-correlation functional. The spectra are convoluted by a Gaussian of  $\text{fwhm} = 0.3$  eV.

calculations using the DFT frozen ground state wave functions (DFT-Frozen), we note that by large the outcome is the same, except for the oxygen  $5\sigma$  level which now obtains intensity comparable to that of the  $4\sigma$  in agreement with experiment (Table 3 and Figure 2a,b). One thus arrives at the somewhat ironic conclusion that the lower order theory is better, something that in this case has an important ramification in that the new bonding model proposed on the basis of X-ray emission spectra<sup>1</sup> assumes the ground state frozen orbital model.

Figure 3, we compare DFT and HF results for the CO and CO/Cu<sub>14</sub> systems using intensities computed from frozen ground state wave functions. For free CO one notices only slight changes, while for the cluster there are more noticeable changes especially in the carbon spectrum, with the DFT calculations reproducing the experiment<sup>31</sup> very well concerning both energies and intensities. Similar cluster convergence<sup>15</sup> is obtained with the two methods.

High-energy structures receive quite moderate intensity, in both the carbon and the oxygen XE spectra, but can nevertheless be used for assigning the 4 eV binding energy features observed by Nilsson et al.<sup>30,31</sup>

The results show a very low sensitivity to the choice of exchange-correlation functional; both energy positions and the  $4\sigma/5\sigma$  intensity ratio are well reproduced for all functionals when the ground state orbitals are used for the calculation of the intensities. Thus, only a minor improvement is observed when going from the local density approximation to the gradient-corrected functionals. However, some inclusion of correlation seems to be required in order to obtain the correct intensity

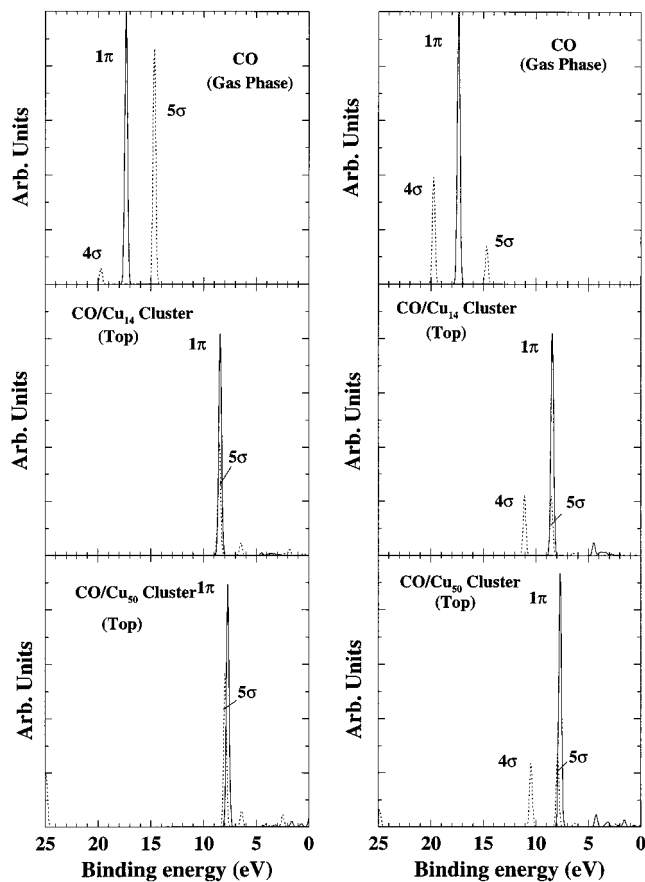


**Figure 2.** Theoretical C(1s) and O(1s) XES spectra computed from DFT in the frozen orbital approximation with Cu–C distance of  $3.51 a_0$  and PD91 exchange-correlation functional. The spectra are convoluted by a Gaussian of  $\text{fwhm} = 0.3$  eV.

ratio as evidenced by the poorer agreement using HF at the frozen orbital level (Figure 3b).

Finally, we note from Table 4 the very good agreement with experiment for the valence binding energies of the CO molecule adsorbed on the Cu<sub>14</sub> cluster. In the table all energies have been corrected for the experimental work function, 4.59 eV,<sup>33</sup> of Cu(100). The  $\Delta\text{SCF}$  values strongly overestimate the valence binding energies and, in particular, result in a large separation of the  $5\sigma$  and  $1\pi$  orbitals whereas the DFT result gives a much smaller splitting, in better agreement with experiment.

**C. XES—Ethylene and Ethylene/Cu(110).** As carbon monoxide, ethylene is a molecule which has earlier been analyzed both experimentally and by computations. It has served as the building block for the polyene oligomer series converging to polyacetylene and for the possible build up of exciton features in nonresonant X-ray emission spectra in such an oligomer series. It has thus been investigated both at the frozen and the relaxed orbital levels<sup>34</sup> and also by means of the special Green's functions technique proposed in ref 35. Indeed, initial state (core-hole) relaxation shifts intensity for ethylene from  $\sigma$  to  $\pi$  orbital levels;<sup>34</sup> the  $\sigma$   $1b_{2u}$ ,  $3a_g$ , and  $1b_{3g}$  transitions then become reduced with respect to the  $\pi$   $1b_{3u}$  transition intensity.<sup>34</sup> With two equivalent core sites its spectrum is more perturbed by relaxation than are heterogeneous compounds such as CO. However, a consideration of relaxation does not necessarily lead to a significant improvement when compared to experiment, and in fact the frozen orbital calculations work well. The Green's function results show no qualitative differences in the spectrum of the outer valence orbitals, indicating that the correlation contributions are not overly important.<sup>35</sup>

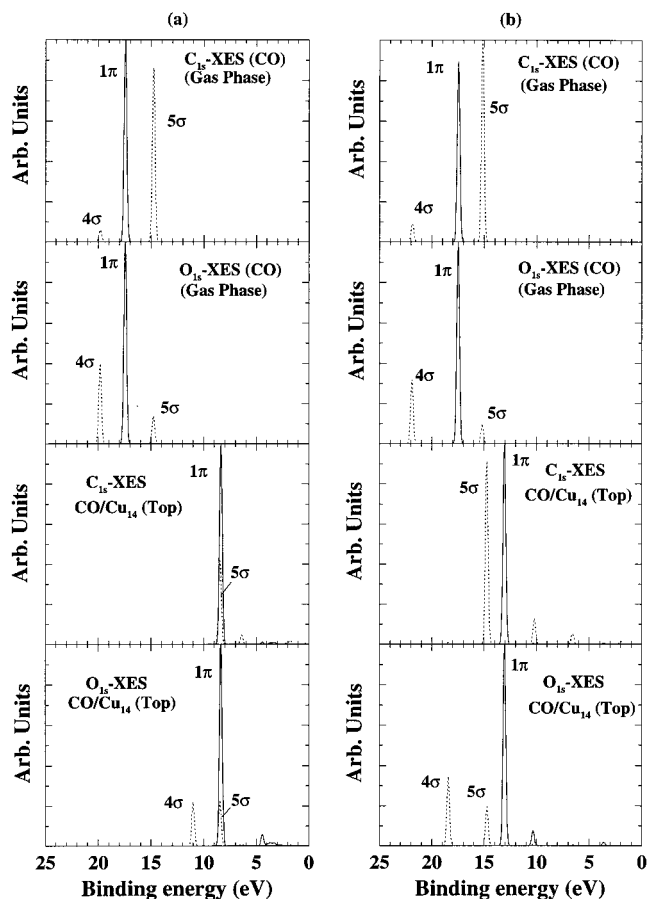


**Figure 3.** Theoretical C(1s) and O(1s) XES spectra computed from both HF (b) and DFT (a) in the frozen orbital picture. The spectra are convoluted by a Gaussian of fwhm = 0.3 eV.

**TABLE 3: Geometries and Spectral Data Computed for Different Exchange and Correlation Functionals for CO Chemisorbed on the Cu<sub>14</sub> Cluster Model of Cu(100)<sup>a</sup>**

funct	geom (a <sub>0</sub> ) <sup>b</sup> CO/Cu <sub>14</sub>	bind. en. (eV)			DFT-Frozen 4σ/5σ
		DFT-Frozen	DFT-TP- ( ε <sub>i</sub> (n <sub>i</sub> <sup>1/2</sup> ) )	DFT-TP 4σ/5σ	
LDA	CO = 2.16	5σ = 7.6	9.7		1.10
	CuC = 3.70	1π = 7.6	8.5	3.18	
		4σ = 9.9	12.0		
BP86	CO = 2.18	5σ = 7.3	8.4		1.06
	CuC = 3.66	1π = 7.4	8.7	3.05	
		4σ = 10.0	11.8		
PW86P86	CO = 2.17	5σ = 7.3	9.0		1.05
	CuC = 3.72	1π = 7.5	8.3	3.40	
		4σ = 10.1	11.9		
PW91	CO = 2.18	5σ = 7.2	9.2		0.99
	CuC = 3.52	1π = 7.1	8.5	2.77	
		4σ = 9.8	11.5		
EXP	CO = 2.19 <sup>c</sup>		5σ = 8.5 <sup>d</sup>		~1.0 <sup>e</sup>
	CuC = 3.60 <sup>c</sup>		1σ = 8.5 <sup>d</sup>		
			4σ = 11.5 <sup>d</sup>		

<sup>a</sup> 4σ/5σ indicates the 4σ to 5σ intensity ratio. <sup>b</sup> Optimized geometry. <sup>d</sup> Reference 44. <sup>e</sup> Reference 45.

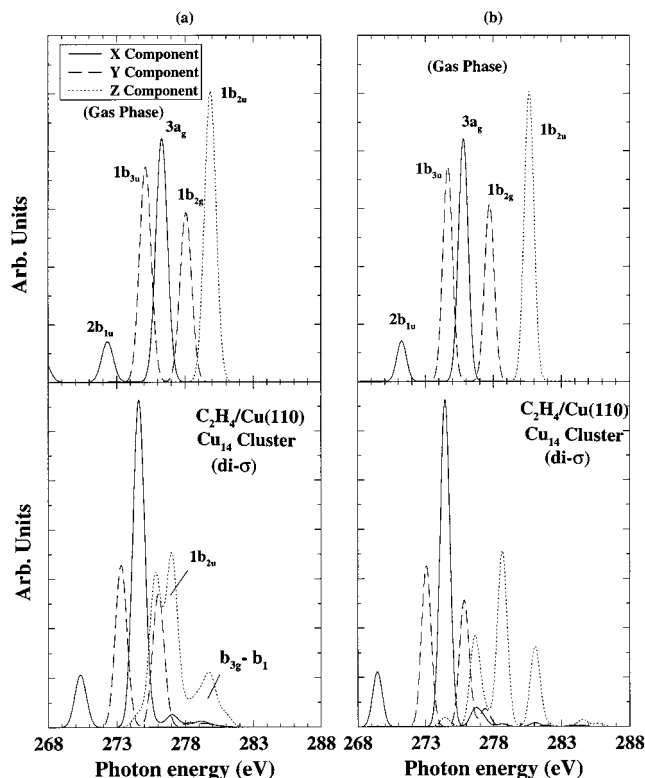
The ethylene/Cu(110) cluster model has the ethylene chemisorbed in the di-σ orientation, with the ethylene molecule placed with the C–C axis parallel to the nearest Cu–Cu neighbor pair on the substrate. For this surface, the C–C distance becomes 1.39 Å, which is 0.06 Å larger than the corresponding C–C distance in the gas-phase ethylene molecule, while the hydrogens move upward from the surface.<sup>18</sup>

Figure 4a shows the spectrum of di-σ-bonded ethylene on Cu(110) obtained from DFT frozen orbital calculations on the

**TABLE 4: Computed Valence Orbital Binding Energies (eV) for CO/Cu<sub>14</sub><sup>a</sup>**

orbital	expt	ε <sub>i</sub> (n <sub>i</sub> <sup>1/2</sup> )	ε <sub>i</sub> (n <sub>i</sub> <sup>1/2</sup> )			ΔSCF	KT
			C	O	Δ		
5σ	8.5	9.0	8.9	8.5	0.4	11.8	14.6
1π	8.5	8.3	9.3	9.9	0.6	9.7	12.9
4σ	11.5	11.9	12.0	12.5	0.5	15.2	18.2

<sup>a</sup> Comparison with Hartree–Fock approach and experimental UPS values from ref 31. All values corrected for the work function of Cu(100), 4.59 eV.<sup>33</sup> See Table 2 for nomenclature.



**Figure 4.** Computed HF and DFT frozen orbital C(1s) XES spectra for ethylene; gas-phase and chemisorbed on Cu(110) in the di-σ adsorption site. The factor of 1.2 for compressing the spectral width has been used for the Hartree–Fock values.<sup>36,46</sup>

C<sub>2</sub>H<sub>4</sub>/Cu<sub>14</sub> cluster. The spectrum is resolved in the x, y, and z directions of the emitted X-ray photons. One observes a population of the b<sub>3g</sub> level which is unoccupied in the gas-phase molecule but also that the occupied π (1b<sub>2u</sub>) level is strongly perturbed and split into two substates by the presence of the cluster.

Important in the present context is to note the successful application of the DFT frozen orbital approach for the intensities. One should then also observe that the Hartree–Fock description is acceptable for this system as it does not deviate significantly from the DFT nor from the experimental results.

As seen in Table 5, the transition energies are extremely well represented by the DFT-TP ε<sub>i</sub>(n<sub>i</sub><sup>1/2</sup>) results; only for the 2b<sub>1u</sub> transition of C<sub>2</sub>H<sub>4</sub> can one note a deviation from experiment by more than 0.3 eV. The ε<sub>i</sub>(n<sub>i</sub><sup>1/2</sup>) energies are notoriously ca. 0.7–1.0 eV too large, indicating that this DFT-TP is too attractive for valence ionization. The Koopman's theorem values are mostly too large and show the typical exaggeration of the full spectral width.

**D. Benzene/Cu(110).** As shown in recent work,<sup>8,18</sup> geometry optimization by the DFT method of benzene on Cu(110) results in two stable chemisorbed structures: an inverted boat quinoid

**TABLE 5: Ionization Potential (eV) for Valence Orbitals and X-ray Emission Energies (eV) for Ethylene Computed in Both DFT-TP and Hartree–Fock Approaches<sup>a</sup>**

orbital	expt	$ \epsilon_i(n_i^{1/2}) $ $ \epsilon_i(n_{1s}^{1/2}) $		$\Delta_2C$	KT	DFT IP <sub>1s</sub> – $ \epsilon_i(n_i^{1/2}) $
		C <sub>2</sub> H <sub>4</sub> , gas phase				
1 $\pi$	10.51	10.78	11.9	–1.1	10.4	279.82
2b <sub>2g</sub>	12.85	12.58	13.1	–0.5	13.8	278.02
3a <sub>g</sub>	14.66	14.58	15.3	–0.7	16.1	276.02
1b <sub>3u</sub>	15.87	15.62	16.3	–0.7	17.5	274.98
2b <sub>1u</sub>	19.10	18.44	19.1	–0.7	21.5	272.16

<sup>a</sup> C<sub>2v</sub> symmetry. <sup>b</sup>  $\Delta_2C = \Delta(\epsilon_i(n_i^{1/2}) - \epsilon_i(n_{C1s}^{1/2}))$ . IP<sub>1s</sub><sup>C</sup> = 290.6 eV (see ref 6).

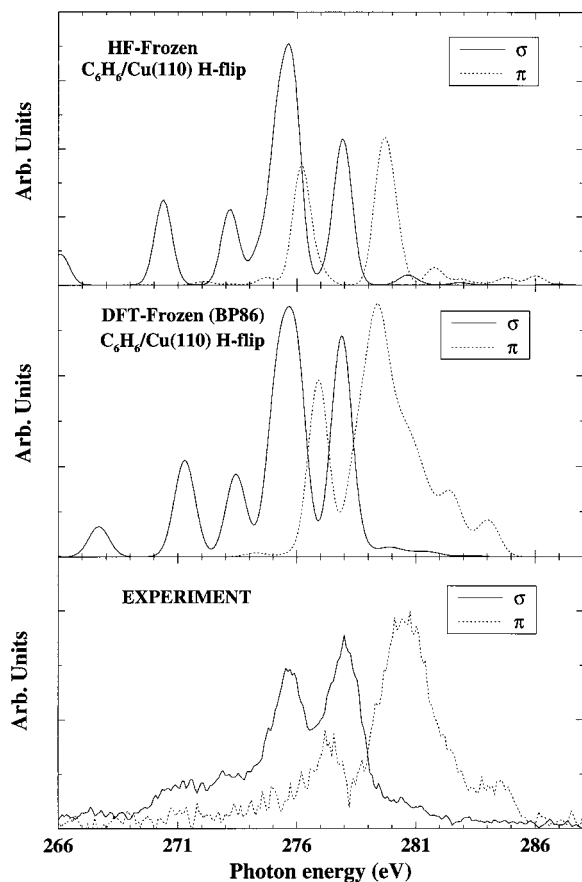


**Figure 5.** Computed HF and DFT frozen orbital C(1s) XES spectra for benzene: gas-phase and chemisorbed on Cu(110). The factor of 1.2 for compressing the spectral width has been used for the Hartree–Fock values.<sup>36,46</sup>

conformation and a planar carbon ring structure with hydrogens flipping upward. In the first conformation, the bending of the carbon plane is predicted to be 7.4°, with four C–C bonds prolonged by 0.05 Å, while the top-plane carbon and hydrogen atoms keep their bond lengths intact. In the second structure, which is only 4 kcal/mol less stable, the C–C bond length was only slightly (0.02–0.03 Å) elongated compared to gas phase but with the C–H bending angle for four hydrogens similar to that for the boat structure. This internal adsorbate restructuring was shown to have particular implications for the character of the spectra computed at the Hartree–Fock level both in absorption and emission.

Simulations indicated that the experiment of ref 1 (giving the X-ray spectrum here reproduced in the lower panel of Figure 5) measured the H-flip form of the adsorbed benzene. Comparison with experiment indicates that this “H-flip” structure can generate both  $\sigma$ – $\pi$  symmetry breaking and angular de-

pendence in the XE spectra in good agreement with experiment; the more strongly distorted inverted boat form results in stronger perturbations of the electronic structure. For the “H-flip” structure, the  $\sigma$  intensity propagates somewhat upward in the spectrum, indicating a weak participation in the surface bonding; see Figure 5. The comparison is obtained at a frozen orbital level of approximation and thus reflects the actual (local) electronic structure. The relaxed orbital picture (see ref 8 for details) gave some smaller “corrections” which, however, do not necessarily seem to improve the experimental comparison.

The assignment of the X-ray emission spectra in Figure 5 is easily given in terms of molecular orbital (MO) theory; we refer to refs 1 and 36. The figure also gives a comparison of DFT frozen orbital calculations with the corresponding Hartree–Fock calculations. The surface orthogonal detection of planar benzene reflects  $\sigma$  orbital emission while surface parallel detection reflects  $\pi$  orbital emission.

The computed XE spectra for chemisorbed benzene are similar to those of the gas phase on a coarse scale. On a finer scale one can observe effects of degeneracy lifting and of a slight overlap of the  $\sigma$ – $\pi$  parts of the spectrum; especially the “ $\sigma$ ” orbital emission is pushed up in the spectrum. At the energy of the 1e<sub>1g</sub> highest occupied molecular orbital (HOMO) there is thus some underlying  $\sigma$  emission for the chemisorbed benzene species. Furthermore, high-energy bands appear in the  $\sigma$  and  $\pi$  parts. For chemisorbed distorted benzene, there is intensity in the gap between the 1e<sub>1g</sub> and the 1e<sub>2u</sub> levels as well as intensity for the 1e<sub>2u</sub> level itself. There are also small background  $\sigma$  contributions in this part of the spectrum. Both the calculations and the experiment indicate that “ $\sigma$ ” bonds participate in the adsorption of benzene.

As shown in ref 8, with the inclusion of orbital relaxation one obtains a spectrum which differs fairly little in the “bound” part but which enhances the e<sub>2u</sub>-derived transitions and the overall  $\pi$  versus  $\sigma$  electron emission, while the internal  $\sigma$  spectrum largely remains intact. By large, the DFT and the HF spectra are quite similar: HF suppresses more the  $\sigma$  3e<sub>3g</sub> level from the gas-phase intensity, in better agreement with experiment, while DFT gives a more complete spectrum in the high-energy  $\pi$  region and a better experimental agreement in that region. This is also the energy region where 3d interactions are expected and which are notoriously poorly described at the HF level of theory.

It is instructive to use the benzene spectra to analyze the effect of relaxation on the XES spectrum. Figure 6 shows a comparison of spectra of the C<sub>6</sub>H<sub>6</sub>Cu<sub>13</sub> cluster, where the benzene ring is corrupted to a boat structure<sup>8</sup> (note that in Figure 5 a H-flip structure was analyzed). The comparison includes frozen orbital and core-hole relaxed orbital calculations and a calculation in which the core excited state was optimized explicitly with a  $\pi^*$  electron present.

With inclusion of orbital relaxation one obtains a spectrum which differs fairly little in the “bound” part, but which enhances the  $\pi^*$  (e<sub>2u</sub>)-derived transitions (e<sub>2u</sub> is the lowest unoccupied molecular orbital (LUMO) in free benzene). As seen by comparing parts a and c of Figure 6, the primary role of relaxation is to enhance the ratio of  $\pi$  versus  $\sigma$  electron emission, while the internal  $\sigma$  spectrum largely remains intact. In the relaxed calculation the initial state is the fully relaxed core-hole state, while for the final valence hole state the frozen ground state orbitals are used in combination with energies from Koopman’s theorem.

In the present calculations we obtain a signal from the “ $\pi^*$ ” band in the frozen orbital approximation due to the slight

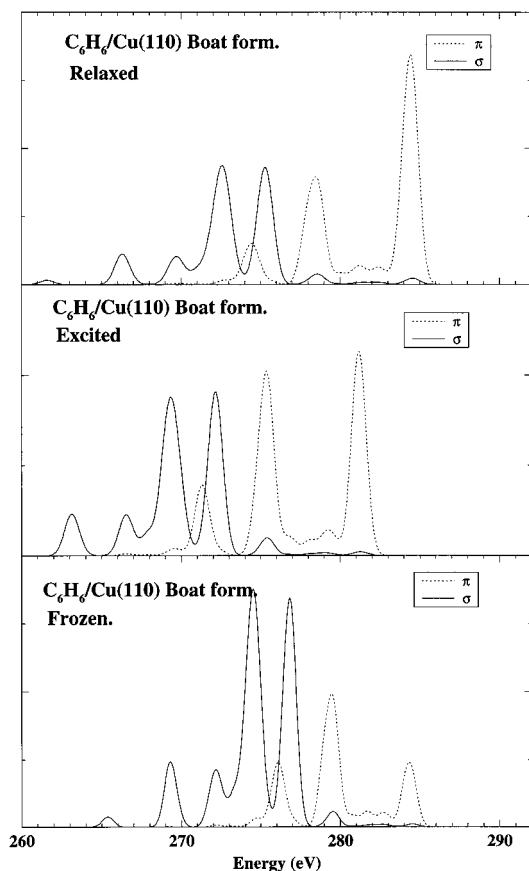


**Figure 6.** Simulated X-ray emission spectra of surface-adsorbed benzene (boat form) with different treatment of relaxation effects:<sup>8</sup> (a) fully relaxed core hole, (b) fully relaxed core hole in the presence of  $\pi^*$  excitation, (c) frozen (unrelaxed) core orbitals. Spectral lines are convoluted with Gaussians with  $\text{fwhm} = 1.0$  eV.

population of the  $e_{2u}$ -derived level in the ground state; this signal, however, increases quite drastically in the relaxed orbital approximation. Thus in the nonresonant model this level is populated by surface screening rather than by excitation as would be the case in a resonant model. For the surface-adsorbed benzene it seems that the excited electron and surface-derived states participate strongly in the screening. Comparing spectra in Figure 6 one sees a large effect on the  $\pi$  state at the Fermi level from removal of the excited electron, which clearly indicates both that the excitation itself can provide screening and that contributions from charge-transfer processes are of importance.

The screening intensity obtained by the relaxed nonresonant model seemingly overestimates the intensity of the emission intensity of the  $\pi^*$  level itself; an observation in common with, for example, results for CO on copper.<sup>15</sup> Apart from the shortcomings in the modeling of the  $\pi^*$  emission, one must here account for the quite different natures of inelastic and elastic scattering processes, as one can expect from the experience with free atoms and molecules.

**E. XES of the N/Cu<sub>61</sub> Cluster.** The chemisorption properties of first-row atoms on metal surfaces have been of great theoretical interest to calibrate different approaches to chemisorption and to investigate the degree of 3d involvement in the bonding. In the particular case of N/Cu(100) we have recently investigated the contribution to the binding energy from dynamical correlation involving the 3d shell and have found very large contributions; the difference between a simple valence (including the adsorbate and Cu 4s) correlation scheme and a

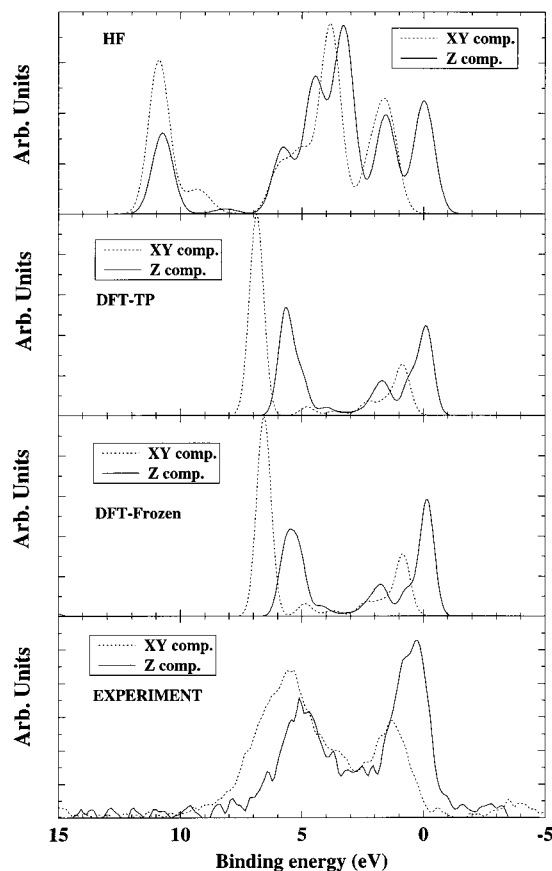


**Figure 7.** Computed and experimental angular resolved XE spectra for N/Cu(100): comparison of different approaches.

calculation with 3d correlation included was of the order of 60 kcal/mol.<sup>37</sup> This energetic effect was accurately given within the gradient-corrected DFT framework, and we have followed up on this success by computing NEXAFS and XES spectra for N/Cu(100).<sup>7</sup> Since this provides a particularly illustrative example of the strength of the DFT approach when dynamical correlation must be included, we will briefly discuss the results for the largest, Cu<sub>61</sub>, cluster model here and also the extension to the frozen DFT picture.

The experimental emission spectrum for  $c(2 \times 2)$  N/Cu(100) (Figure 7) shows two strong peaks both in grazing and normal emission. In the normal emission spectrum ( $p_{x,y}$ ) the main peak is located at 5.46 eV binding energy with the second, less intense, peak at 1.35 eV. In grazing emission ( $p_{z,x}, p_{z,y}$ ) the peaks are in reverse intensity ratio compared with the intensity in normal emission: the  $p_z$  spectrum has almost twice the intensity in the lower-energy peak. The energy difference between the peaks is close to 5 eV in both cases, but with a difference in peak position between the  $p_{x,y}$  and  $p_z$  spectra of 0.6 eV (low-energy peak) and 0.9 eV (high-energy peak) with the  $p_z$  peaks always at higher energy. Both the grazing and normal spectra are very well reproduced by the DFT-TP approach, while the HF-STEX completely fails to reproduce even the qualitative aspects of the orbital structure. This is due to the strong interaction with the 3d shells and covalent bond formation between N2p and Cu3d; in a theoretical treatment this requires dynamical correlation to be included to compensate the loss of exchange interaction within the strongly coupled 3d shell. From the correlation contribution to the chemisorption energy it is already clear that the Hartree-Fock picture leaves out main components of the bonding, but these are very well recapitulated

by the DFT-TP approach, including the changes to the occupied molecular orbitals, as evidenced from the computed spectra.

In the present work we have also computed the N(1s) emission spectra for the N/Cu(100) surface in the frozen orbital picture implemented in the DFT framework (see Figure 7); the spectra have been aligned on the binding energy scale from the DFT-TP calculations. The bonding picture does not change when comparing with the DFT-TP approach. The normal emission spectra ( $p_{x,y}$ ) also remains almost the same, while in the grazing emission spectra we can see an improvement in the intensity ratio using DFT-Frozen, toward a better correspondence with the experiment.

**F. Frozen versus Relaxed Orbital Pictures.** As pointed out in the previous text, the frozen orbital picture is favorable for evaluation of XES intensities despite the fact that an unoccupied  $\pi^*$  level can undergo a heavy population during the creation of the initial core hole. The XES spectra from the screening  $\pi^*$  level itself shows, on the other hand, a strong variation between relaxed and frozen orbital treatments as discussed in section III.D. and shown in Figure 6. This can be discussed in light of the theory of Mahan,<sup>38</sup> Nozieres, and DeDominicis<sup>39</sup> (MND) for the dynamics of the core-hole state; see also a review on the soft X-ray edge problem by Ohtaka and Tanabe.<sup>40</sup> According to the MND theory, the role of the core-hole relaxation is large for metals because of the absence of a gap between occupied and unoccupied states. The core hole creates electron-hole pairs (shake-up pairs) with the largest probability for states lying close to the Fermi level, and, as a result, in the field of a core hole there is a strong reconstruction of the Bloch states close to the Fermi level.

Another consequence of the absence of a gap between occupied and unoccupied states is a strong change of the matrix elements for the emission transitions from the states close to the Fermi level. However, the role of this relaxation effect is small for Bloch states lying further below the Fermi level: at approximately  $<0.1D$ , where  $D$  is the width of the valence band, it is negligible. According to numerical calculations in ref 40, the spectral shape of the emission transitions from these states coincide with good accuracy with those obtained from the frozen orbital approximation. When the lifetime broadening of the core excited state increases, the MND singularities close to the Fermi surface decrease and the frozen orbital approximation works better. One can say "that the Bloch states have no time to relax" if the lifetime of the core excited state is short.

In the case of finite band gaps the role of particle-hole (shake-up) excitations induced by the core hole will be weaker in terms of perturbation on the wave function but will, on the other hand, involve a larger portion of the occupied band, also below  $0.1D$ . In molecules having large excitation gaps, core-hole-induced relaxation a priori not be disregarded for any level; the outcome of the relaxation is then more dependent on the particular localization of the levels with respect to the core hole. For the role of initial and final state relaxation and electron correlation in XES spectra of free molecules, we refer to refs 41 and 27.

It is interesting to note that the simulations of XES spectra of surface adsorbates presented in this work seem to concord with MND theory in that most of the core-hole induced relaxation effects are located to the outermost screening  $\pi^*$  level, while other occupied levels seemingly are well described by the frozen orbital calculations. In this sense the surface adsorbate spectra behave more metallic-like than molecular-like. More simulations and systems are evidently required to make a firm conclusion of this point.

## IV. Conclusions

Following a related proposal for NEXAFS spectroscopy,<sup>6</sup> we have in this work presented and analyzed results from calculations of X-ray emission spectra using density functional theory in combination with ground state (frozen orbital) and transition potential approaches. For XES we obtain spectra which are of Hartree–Fock or even MCSCF/CI quality. As with Hartree–Fock, the calculations simulating surface adsorbates show good convergence with increasing cluster size, and the comparison with Hartree–Fock generally comes out quite well concerning intensities, while energies often are improved by DFT-TP. Special cases, however, such as atomic nitrogen adsorption on copper, require a DFT description to obtain even qualitative experimental agreement concerning both intensities and energies. Such cases demonstrate the need to have proper positioning of metal bands versus the energy levels of the free adsorbate molecule and also the proper correlation treatment to account for the strong interaction with the 3d shell and covalent bond formation with the  $Cu_{3d}$  band. Calculations of weaker fine structures at high energies, which are quite dependent on surface bonding, also seem to be better represented in the DFT-based formalism.

We find the use of final state transition potentials and a common valence IP energy scale to work very well for predicting the XES energies. For free molecules, this gives experimental agreement on a subelectronvolt scale even for absolute energies and is actually not much worse for the surface adsorbates. An example studied in some detail here, namely CO/Cu(100), shows energies very close to those experimentally observed. The core DFT-TP model is computationally favorable in that a full spectrum, energies and intensities, is obtained in one calculation, but it has the disadvantage of giving different energies for different core-sited spectra (like C and O spectra of CO) when put on the common, valence IP, energy scale. For example, the difference of the  $1\pi$  bands derived from O1s and C1s DFT-TP calculations is as large as 1 eV for CO/Cu(100).

Concerning intensities it is found that the frozen orbital approximation (DFT-Frozen) works well and seemingly better than using core DFT-TP orbitals: The  $5\sigma/4\sigma$  intensity ratio in the oxygen spectra of CO/Cu(100) is a conspicuous case for which experimental agreement was obtained *only* at the frozen level. The relaxation thus does not necessarily improve upon frozen calculations, a fact which may be due to an unbalanced treatment of relaxation in the initial and final states when only initial state relaxation is included, as in the transition potential implementation or the relaxed Hartree–Fock calculation. Similar effects of cancellation of initial and final state contributions are well known, e.g., for valence state binding energies as exemplified by the balance of the relaxation (final state) and correlation (initial state) corrections to the Koopman's theorem IPs. However, for core ionization, relaxation produces 1 order of magnitude larger contributions than those for the valence ionizations, and one would from that outset expect improvements in calculated XE intensities using relaxed  $\Delta$ SCF or the transition potential approaches either in Hartree–Fock or DFT. Contrary to the NEXAFS, for which the use of core-hole relaxed orbitals is mandatory, the present study indicates that this is not the case for X-ray emission; it seems that the surface adsorbate species behave more metallic-like than molecular-like in this respect. We refrain from further speculations on that point and end this study by concluding that the support from simulations of the ground state model to interpret XE spectra has an obvious and important ramification for the use of this

technique to analyze the bonding and other *ground state* properties of surface adsorbates.

**Acknowledgment.** Valuable discussions with A. Nilsson are gratefully acknowledged. We are grateful for the consent to reproduce the experimental spectra and thank T. Wiell and P. Bennich for assistance in preparing the figures. We also acknowledge the authors of ref 1 for useful discussions and for providing their XES spectra of C<sub>6</sub>H<sub>6</sub>/Cu(110).

## References and Notes

- (1) Nilsson, A.; Wassdahl, N.; Weinelt, M.; Karis, O.; Wiell, T.; Bennich, P.; Hasselström, J.; Fölich, A.; Stöhr, J.; Samant, M. *Appl. Phys. A* **1997**, *65*, 147.
- (2) Nilsson, A.; Weinelt, M.; Wiell, T.; Bennich, P.; Karis, O.; Wassdahl, N.; Stöhr, J.; Samant, M. *Phys. Rev. Lett.* **1997**, *78*, 2847.
- (3) Stener, M.; Lisini, A.; Decleva, P. *Chem. Phys.* **1995**, *191*, 141.
- (4) Hu, C. H.; Chong, D. P. *Chem. Phys. Lett.* **1996**, *262*, 729.
- (5) Hu, C. H.; Chong, D. P. *Chem. Phys. Lett.* **1996**, *249*, 491.
- (6) Triguero, L.; Pettersson, L. G. M.; Ågren, H. *Phys. Rev. B*, in press.
- (7) Triguero, L.; Pettersson, L. G. M. *Surf. Sci.* **1998**, *398*, 70.
- (8) Pettersson, L. G. M.; Ågren, H.; Luo, Yi; Triguero, L. *Surf. Sci.*, in press.
- (9) Salahub, D. R.; Fournier, R.; Mlynarski, P.; Papai, I.; St-Amant, A.; Ushio, J. In *Density Functional Methods in Chemistry*; Labanowski, J., Andzelm, J., Eds.; Springer: New York, 1991; p 77. St-Amant, A. Ph.D. Thesis, Université de Montréal, 1992. The present version of the program has been substantially modified by L. G. M. Pettersson.
- (10) Slater, J. C. *Quantum Theory of Molecules and Solids*; McGraw-Hill: New York, 1974; Vol. IV.
- (11) Chong, D. P. *Chem. Phys. Lett.* **1995**, *232*, 486.
- (12) Stöhr, J. *NEXAFS Spectroscopy*; Springer-Verlag: Berlin, 1992.
- (13) Siegbahn, H.; Medeiros, R.; Goscinski, O. *J. Electron Spectrosc. Relat. Phenom.* **1976**, *8*, 149.
- (14) Almlöf, J.; Faegri, K., Jr.; Feyereisen, M.; Korsell, K. DISCO, a direct SCF and MP2 code.
- (15) Pettersson, L. G. M.; Ågren, H.; Vahtras, O.; Carravetta, V. *Surf. Sci.* **1996**, *365*, 581.
- (16) Dunning, T. H., Jr. *J. Chem. Phys.* **1971**, *55*, 716.
- (17) Huzinaga, S. *J. Chem. Phys.* **1965**, *42*, 1293.
- (18) Triguero, L.; Pettersson, L. G. M.; Minaev, B.; Ågren, H. *J. Chem. Phys.* **1998**, *108*, 1193.
- (19) Perdew, J. P.; Wang, Y. *Phys. Rev. B* **1986**, *33*, 8800.
- (20) Perdew, J. P. *Phys. Rev. B* **1986**, *34*, 7406.
- (21) Perdew, J. P. *Phys. Rev. B* **1986**, *33*, 8822.
- (22) Seminario, J. M.; Politzer, P. *Density Functional Theory. A Tool for Chemistry*; Elsevier Science B. V.: Amsterdam, 1995.
- (23) Becke, A. D. *Phys. Rev. A* **1988**, *38*, 3098.
- (24) Vosko, S. H.; Wilk, L.; Nusair, M. *Can. J. Phys.* **1980**, *58*, 1200.
- (25) Wachters, A. J. H. *J. Chem. Phys.* **1970**, *52*, 1033.
- (26) Mattsson, A.; Panas, I.; Siegbahn, P.; Wahlgren, U.; Åkeby, H. *Phys. Rev. B* **1987**, *36*, 7389.
- (27) Ågren, H.; Flores-Riveros, A. J. *Electron Spectrosc. Relat. Phenom.* **1991**, *56*, 259.
- (28) Ågren, H.; Arneberg, R. *Phys. Scr.* **1983**, *28*, 80.
- (29) Skytt, P.; Glans, P.; Gunnelin, K.; Guo, J.-H.; Nordgren, J.; Luo, Y.; Ågren, H. *Phys. Rev. A* **1997**, *55*, 134.
- (30) Nilsson, A.; Bennich, P.; Wiell, T.; Wassdahl, N.; Mårtensson, N.; Nordgren, J.; Björneholm, O.; Stöhr, J. *Phys. Rev. B* **1995**, *51*, 10244.
- (31) Bennich, P. Ph.D. Thesis, Uppsala University, Sweden, 1996.
- (32) Wassdahl, N.; Nilsson, A.; Wiell, T.; Tillborg, H.; Duda, L. C.; Guo, J. H.; Mårtensson, N.; Nordgren, J.; Andersen, J. N.; Nyholm, R. *Phys. Rev. Lett.* **1994**, *69*, 812.
- (33) Heskett, D.; Strathy, I.; Plummer, E. W.; de Paola, R. A. *Phys. Rev. B* **1985**, *32*, 6222.
- (34) Gel'mukhanov, F.; Yang, L.; Ågren, H. *J. Chem. Phys.* **1996**, *105*, 5224.
- (35) Liegener, C. M.; Ågren, H. *J. Chem. Phys.* **1993**, *99*, 2821.
- (36) Skytt, P.; Guo, J. H.; Wassdahl, N.; Nordgren, J.; Luo, Y.; Ågren, H. *Phys. Rev. A* **1995**, *52*, 3572.
- (37) Triguero, L.; Wahlgren, U.; Pettersson, L. G. M.; Siegbahn, P. *Theor. Chim. Acta* **1996**, *94*, 297.
- (38) Mahan, G. D. *Phys. Rev.* **1967**, *163*, 612.
- (39) Nozieres, P.; De Dominicis, C. T. *Phys. Rev.* **1969**, *178*, 1097.
- (40) Ohtaka, K.; Tanabe, Y. *Rev. Mod. Phys.* **1990**, *62*, 929.
- (41) Ågren, H.; Flores-Riveros, A.; Jensen, H. J. Aa. *Physica Scripta* **1989**, *40*, 745.
- (42) Carravetta, V.; Pettersson, L. G. M.; Ågren, H.; Vahtras, O. *Surf. Sci.* **1996**, *369*, 146.
- (43) Chong, D. P.; Langhoff, S. R. *J. Chem. Phys.* **1986**, *84*, 5606.
- (44) McConvill, C. F.; Woodruff, D. P.; Prince, K. C.; Paolucci, G.; Chab, V.; Surman, M.; Bradshaw, A. M. *Surf. Sci.* **1986**, *166*, 221.
- (45) Nilsson, A.; et al. Manuscript in preparation.
- (46) Ort'i, E.; Brédas, J. L. *J. Chem. Phys.* **1988**, *89*, 1009.